Interpretable Data-Driven Modeling in Biomass Preprocessing

Daniel L. Marino [1], Matthew Anderson [2], Kevin Kenney [2], Milos Manic [1]
[1] *Virginia Commonwealth University, Richmond, Virginia*
[2] *Idaho National Laboratory, Idaho Falls, Idaho*
marinodl@vcu.edu, matthew.anderson@inl.gov, misko@ieee.org

***Abstract*—Data-driven models provide a powerful and flexible modeling framework for decision making and controls in industry. However, extracting knowledge from these models requires development of easily interpretable visualizations. In this paper, we present a data-driven methodology for modeling and visualization of relative equipment workload in a biomass feedstock preprocessing plant. The methodology is designed to serve in two main fronts: (1) knowledge discovery and data-mining from instrumentation data, (2) improving situational awareness during monitoring and control of the plant. We used Gaussian Processes to create a model of the expected current overload rate of for each of the electric motors involved in the plant. The expected number of overloads on each equipment was used to quantify and visualize the relative workload of the different components of the system. The visualization is presented in the form of an intuitive directed graph, whose properties (node size, position, colors) are driven by overload rates estimations.**

***Index Terms*—Biomass, Feedstock pre-processing, Gaussian Processes, Graph Visualization**

I. Introduction

Data-driven models provide powerful modeling and analysis tools for large and complex industrial systems [1] [2] [3] [4]. From a data-analysis perspective, intuitive data visualization techniques are essential for extracting knowledge from data. Visual data exploration is essential to formulate hypothesis about the underlying distributions of the data [5] [6]. Visualizations are also an essential tool for understanding data-driven black-box models [7]

In this paper, we present a methodology for estimating and visualizing the workload on different components of a biomass preprocessing plant. The system was developed for the Biofuels National User Facility Preprocessing Process Demonstration Unit (PDU), operated by the Idaho National Laboratory (INL).

Figure 1 shows a simplified diagram of the PDU. The plant consist of a two stage grinding process (Grinder G1 followed by Grinder G2) with a series of drag conveyors and screw conveyors to transport material being processes. A more detail description can be found in [4].

The PDU performs mechanical size reduction of biomass feedstock. Size reduction is a fundamental step for the production of biofuels [4]. This process helps to increase the bulk density [8], [9], reduce transportation and storage costs [9] [10] [11], and influences pellet durability and densification processes [12]. Size reduction is also required for most of biomass refinery and combustion technologies [13] [14] [10].

Biomass feedstock presents large variability in terms of moisture content, ash and particle morphology [15]. The high variability on the feedstock properties affects the performance of the grinding process [9] [15] [4]. As a result, the operation of the PDU is characterized by overloads in the the electric motors current. These overloads are commonly used by the engineers at the PDU plant to quantify the workload on the different equipments.

In this paper, we extend on the work presented in [16] [4]. In [16] a set of fuzzy rules is used to create a relevance score for the main components of the PDU. The scores are used to create a directed graph representation of the system. This methodology provides an intuitive representation of the system. However, the design of the fuzzy rules used in [16] can be an exhaustive and subjective process.

In this paper, we replaced the relevance score from [16] with a Softmax over the predictions of a Gaussian Process (GP). The Softmax provides an intuitive output that takes the form of a multinomial probability distribution. With this approach, a score in the range $[0, 1]$ is assigned to each component of the PDU. The score obtained by the Softmax is then introduced in an optimization program to obtain a set of scales.

The presented visualization consists of a directed graph whose properties (node size, color, node positions) are proportional to the set of scales obtained from the optimization program. These properties provide an effective way to attract and focus the attention of the user by displaying the most relevant information in an intuitive way [17] [16] [18]. The estimation of the GPs are also presented using contour plots, providing a visualization of the estimations for the individual components, trend of the data, and confidence of the estimations [4].

The visualization provides an intuitive way to extract knowledge from data. The visualization also serves as a tool to increase situational awareness [16]. The graph can be used by the operators of the plant to understand the relative workload for a particular plant configuration. Understanding the workload helps the operators to understand the limitations of the system and focus their efforts on the bottleneck of the system.

The rest of the paper is organized as follows: section II presents an overview of the Gaussian Process model used as data-driven mode. Section III describes the presented

978-1-5386-5024-0/18/$31.00

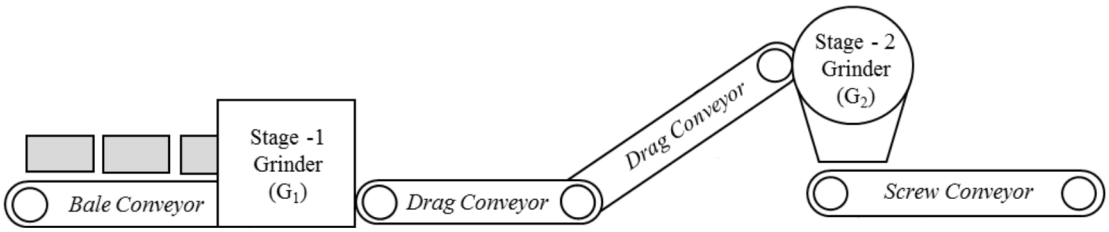

Fig. 1: Process Demonstration Unit (PDU) [4]

methodology for modeling and visualization of the equipment workload. Section IV presents the results of the visualization. Section V concludes the paper.

II. Gaussian Process

Gaussian Processes (GP) [19] are particularly appealing because of their ability to provide estimations of uncertainty. In [4] Gaussian Processes (GP) with linear mean prior were used to model and estimate the response of the PDU to different configurations and control settings.

$$f(\boldsymbol{x}) \sim \mathcal{GP}(\mu(\boldsymbol{x}), k(\boldsymbol{x}, \boldsymbol{x})) \tag{1}$$

Given a set of training $(\boldsymbol{f}, \boldsymbol{X})$ and testing $(\boldsymbol{f}_*, \boldsymbol{X}_*)$ datasets, a GP assumes a Multi-variate normal as prior distribution:

$$\begin{bmatrix} \boldsymbol{f} \\ \boldsymbol{f}_* \end{bmatrix} \sim \mathcal{N}\left(\begin{bmatrix} \mu(\boldsymbol{X}) \\ \mu(\boldsymbol{X}_*) \end{bmatrix}, \begin{bmatrix} \boldsymbol{K} & \boldsymbol{K}_* \\ \boldsymbol{K}_* & \boldsymbol{K}_{**} \end{bmatrix} \right) \tag{2}$$

Where $\boldsymbol{K} = k(\boldsymbol{X}, \boldsymbol{X}) + \sigma_n^2 \boldsymbol{I}$, $\boldsymbol{K}_* = k(\boldsymbol{X}, \boldsymbol{X}_*) = k(\boldsymbol{X}_*, \boldsymbol{X})$, $\boldsymbol{K}_{**} = k(\boldsymbol{X}_*, \boldsymbol{X}_*)$ are matrices obtained by evaluating the Gaussian kernel:

$$k(\boldsymbol{x}, \boldsymbol{x}') = \sigma_f^2 \exp\left(-\frac{(\boldsymbol{x} - \boldsymbol{x}')^2}{2l^2} \right) \tag{3}$$

The posterior distribution is computed as follows [19]:

$$p(\boldsymbol{f}_* | \boldsymbol{X}_*, \boldsymbol{X}, \boldsymbol{f}) = \mathcal{N}(\boldsymbol{f}_* | \boldsymbol{\mu}_*, \boldsymbol{\Sigma}_*) \tag{4}$$

$$\begin{aligned} \boldsymbol{\mu}_* &= \hat{\mu}(\boldsymbol{X}_*, \boldsymbol{X}, \boldsymbol{f}) \\ &= \mu(\boldsymbol{X}_*) + \boldsymbol{K}_*^T \boldsymbol{K}^{-1} (\boldsymbol{f} - \mu(\boldsymbol{X})) \end{aligned} \tag{5}$$

$$\begin{aligned} \boldsymbol{\Sigma}_* &= \hat{\boldsymbol{\Sigma}}(\boldsymbol{X}_*, \boldsymbol{X}, \boldsymbol{f}) \\ &= \boldsymbol{\Sigma}_{**} - \boldsymbol{K}_*^T \boldsymbol{K}^{-1} \boldsymbol{K}_* \end{aligned} \tag{6}$$

Where $\mu(\boldsymbol{X}) = \boldsymbol{X}\boldsymbol{W} + \boldsymbol{b}$ is a linear function that is used to capture the global trend of the system, while the GP captures local behavior [4]

III. Data-Driven Modeling and Visualization

This section presents the novel data-driven modeling and visualization methodology developed for estimating and visualizing the equipment workload on the PDU. Figure 2 shows the diagram of the presented methodology for workload estimation and visualization. The first stage consist on Spike (overload) detection. In the second stage, data from the spike detection algorithm is aggregated to build a dataset. In the third stage, the dataset is used to build a GP model for each one of the components of the plant. The GP provides estimations about the expected rate of spikes that is fed into the visualization algorithm. The visualization stage creates a directed graph whose properties are derived from the expected rate of spikes.

A. Stage 1: Spike Detection

The spike detection algorithm consists of a rolling window that checks if the current has supprased the FLA (full load amperage) for the equipment. Routine 1 presents the rolling window algorithm. RollingWindow calls the SpikeDetection routine (2) which identifies if a spike is present in the window.

Routine (2) uses a non-maxima suppression [20] in order to obtain a single signal when a spike occurs. The non-maxima suppression checks if the value in the middle of the window is the maximum value on the entire window. This serves as an useful tool to identify a spike as a single event.

Routine 1: RollingWindow$\left(I_{[t]}\right)$

Input: Current signal $I_{[t]}$, Window size L
Output: Spikes sequence $\left\{s_{[t]}\right\}$

for $t = 0$ to $|I|$ **do**
  $W \leftarrow \left\{I_{[i]} | t - L \leq i \leq t + L\right\}$
  $S_{[t]} = SpikeDetection(W, I_{[t]})$
end for
return Sequence of spike events $\left\{S_{[t]}\right\}$

Routine 2: SpikeDetection $\left(W, I_{[t]}\right)$

Input: Window W, signal min $I_{\min}$, signal max $I_{\max}$
Output: Spikes sequence $\left\{s_{[t]}\right\}$

if $I[t] = \max(W)$ // non-maxima supression
  and $I_{\max} \leq I[t]$ // FLA threshold
  and $I_{\min} \leq all(W)$ // Ignore start-up
then
  return true
else
  return false
end if

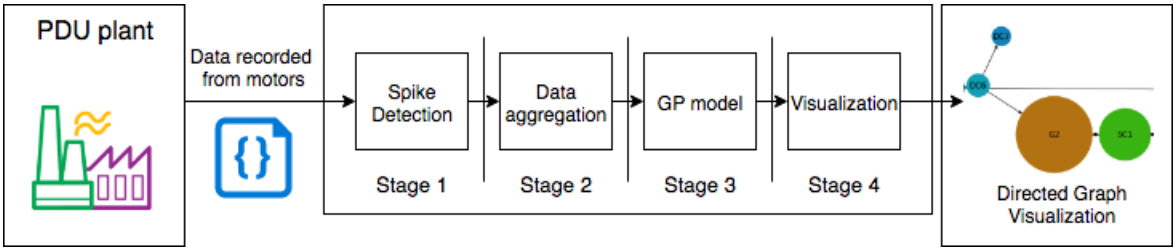

Fig. 2: Overview of the presented methodology

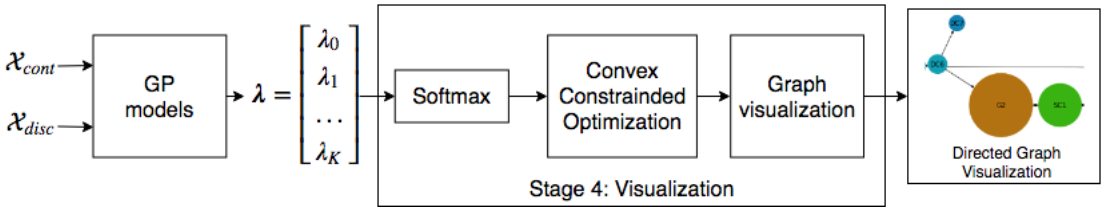

Fig. 3: Visualization Pipeline

B. Stage 2: Data aggregation

The variables used for estimating the rate of spikes are divided into a set of discrete $\mathcal{X}_{disc}$ and continuous $\mathcal{X}_{cont}$ variables:

$$\mathcal{X}_{disc} = \{\text{G1 screen size}, \text{G2 screen size}\} \quad (7)$$

$$\mathcal{X}_{cont} = \{\text{Bale moisture content}, \text{G1 infeed rate}\} \quad (8)$$

$\mathcal{X}_{disc}$ and $\mathcal{X}_{cont}$ are also the decision/control variables for running the system [4]. These variables are kept constant while processing a single bale. This allows us to use aggregate measurements to build the GP models.

The overload rate $\lambda^{[i]}$ experienced during the processing of a bale i is estimated as follows:

$$\bar{\lambda}^{[i]} = \frac{\sum_{t=0}^{T}(s_{[t]})}{T} \quad (9)$$

where $S_{[t]}$ is the sequence of spike events obtained using Routine 1.

C. Stage 3: Gaussian-Process Model

We use Gaussian Processes (GP) with linear mean prior as a data-driven model for estimating the rate of spikes ($\boldsymbol{\lambda}$) for each one of the M motors of the system [19] [4].

The overload rate $\lambda_{[m]}$ for each motor m is modeled using a Gaussian Process. A set of Gaussian Processes $\left\{GP_{[m]}^{[\boldsymbol{x}_{disc}]}\right\}$ is obtained for each combination of motors m and discrete variables $\mathcal{X}_{disc}$:

$$\lambda_m(\boldsymbol{x}_{cont}) = GP_{[m]}^{[\boldsymbol{x}_{disc}]}\left(\mu(\boldsymbol{x}_{cont}), k(\boldsymbol{x}_{cont}, \boldsymbol{x}_{cont})\right)$$

The estimations from the GPs are represented in a compact vector form $\boldsymbol{\lambda}$:

$$\boldsymbol{\lambda} = \begin{bmatrix}\lambda_1 & \lambda_2 & \ldots & \lambda_M\end{bmatrix}^T \quad (10)$$

The training dataset is constructed by computing the aggregated overload rate $\bar{\lambda}^{[i]}$ (Eq. 9) for each one of the bales i in the dataset. For each one of the motors m, the set of tuples $D(m, \boldsymbol{x}_{disc}) = \left\{(\bar{\lambda}[i, m, \boldsymbol{x}_{disc}], \mathcal{X}_{cont}[i, m, \boldsymbol{x}_{disc}])\right\}$ is used to construct a dataset $(\boldsymbol{\lambda}, \boldsymbol{X})$ that is used to train the corresponding $GP_{[m]}^{[\boldsymbol{x}_{disc}]}$ model.

D. Stage 4: Visualization

Figure 3 shows an overview of the presented methodology for visualizing the relative workload on the PDU plant. The visualization consists of a directed graph whose properties are adjusted according to the estimations made by the GP models.

For visualization, we want to clearly visualize the relative workload of each one of the components of the system. The rate of spikes per minute is often used by the engineers at the PDU plant as a measurement of the equipment workload. Therefore, we use the GP estimations of expected spikes rate to estimate the workload of each one of the components. To obtain a relative workload measurement between the components, we apply a Softmax to the estimations of the GP:

$$\sigma(\lambda_m) = \frac{\exp \mathbb{E}\left[\lambda_m\right]}{\sum_j^M \exp \mathbb{E}\left[\lambda_j\right]} \quad (11)$$

The output from the softmax is a proper multinomial probability distribution, whose values are in the range $[0, 1]$ and sum up to one. As the name suggest, the softmax is a soft version of the max operator, assigning a greater value to the largest element of the vector $\boldsymbol{\lambda}$.

The outputs from the softmax can be easily interpretable as relative workload measurements. We use these values to create a visualization of the predicted workload for the system.

The system is visualized using a graph, where each one of the components of the system is represented as a node [16]. In order to provide an easily interpretable visualization, we want the nodes to be scaled according to $\sigma\left(\boldsymbol{\lambda}\right)$.

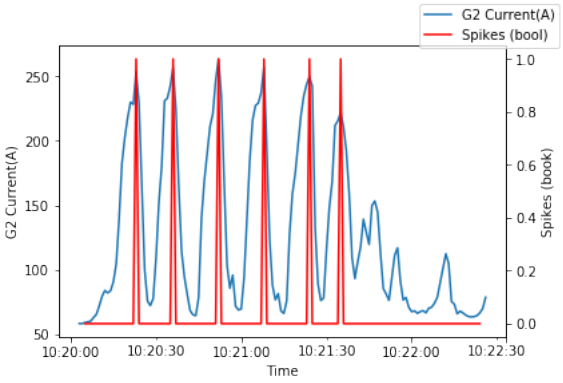

Fig. 4: Spike detection on G2 during the processing of a single bale

The objective of the visualization is to present a graph, where the scales $\boldsymbol{v}$ of the nodes are as close as possible to the relative workload measurement $\sigma(\boldsymbol{\lambda})$. In addition, the scales are desired to have the following constraints: (1) a lower and upper bound over the individual component scales $v_{\min} \leq \boldsymbol{v}_i \leq v_{\max}$, (2) the scales must sum up to one $\mathbf{1}^T\boldsymbol{v} = \sum_m \boldsymbol{v}_m = 1$. The upper and lower bounds ensure that all nodes are visible and do not occupy the entire window. The sum constraint improves interpretability,

We use a cross-entropy to evaluate the difference between the visualization scales $\boldsymbol{v}$ and the relative workload measurement $\sigma(\boldsymbol{\lambda})$

$$H(\sigma(\boldsymbol{y}), \boldsymbol{v}) = -\sum_i \sigma(\boldsymbol{y}_i)\log(\boldsymbol{v}_i) \tag{12}$$

The scales are found using a constrained convex optimization program that minimizes the cross entropy difference 12:

$$\begin{aligned} \min_{\boldsymbol{v}} \quad & H(\sigma(\boldsymbol{y}), \boldsymbol{v}) \\ s.t. \quad & \boldsymbol{v}_{min} \leq \boldsymbol{v} \\ & \boldsymbol{v} \leq \boldsymbol{v}_{max} \\ & \mathbf{1}^T\boldsymbol{v} = 1 \end{aligned} \tag{13}$$

It is important to notice that the cross-entropy is not symmetric, i.e. $H(\sigma(\boldsymbol{y}), \boldsymbol{v}) \neq H(\boldsymbol{v}, \sigma(\boldsymbol{y}))$. For satisfactory results, it is important that the minimization is performed over $H(\sigma(\boldsymbol{y}), \boldsymbol{v})$ and not over $H(\boldsymbol{v}, \sigma(\boldsymbol{y}))$

IV. Results and Discussion

Figure 4 shows an example of the results obtained using the spike detection algorithm from section III-A The figure shows how each spike is detected as a single event, even when the duration of the overload spans over multiple consecutive sample points.

We used the visualization scales $(\boldsymbol{v})$ to create a directed graph diagram of the components of the system. Figure 5 shows the visualization of the graph for screen sizes $\mathcal{X}_{disc} = (3.0, 1.0)$, bale moisture 20% and infeed rate 10%. The nodes of the directed graph represent the electric motors involved in the feedstock size-reduction process. G1U and G1L correspond to the motors present in the first grinder while G2 represents the motor for grinder two. The rest of the nodes represent the motors in the screw (SC) and drag (DC) conveyors that transport the biomass feedstock being processed.

The scales $\boldsymbol{v}$ (Eq. 13) were used to obtain:

- Scales for the nodes
- Position of the nodes
- Color of the nodes

The scales are mapped to colors using the HSV color space. The saturation and value are fixed, and $\boldsymbol{v}$ is used to linearly interpolate between blue (0.0) to orange (1.0)

The vertical positions of the graph were computed using the Fruchterman-Reingold force-directed algorithm algorithm [21]. Given the pipeline arrangement of the PDU plant, the horizontal positions were derived from scales $\boldsymbol{v}$ in incremental order.

We found a good heuristic for setting the parameters v_{max}, v_{min} to be:

$$\begin{aligned} v_{max} &= \frac{A}{K}, \quad A > 2 \\ v_{min} &= 1e^{-5} \end{aligned} \tag{14}$$

where A represents the maximum relative proportion that a particular node can have with respect all other nodes. v_{min} was specified close to zero in order to have strictly positive scales. We found that the $\mathbf{1}^T\boldsymbol{v} = 1$ constraint helped to ensure that the nodes were visible, enforcing that the visualization area was properly covered.

Figure 5b shows the overload rate estimations for the given screen sizes. The confidence contour plot served as a companion tool to the directed graph to visualize the explored space. The confidence plot alerts the operator of possible erroneous predictions [4].

The directed graph visualization (Fig. 5a) shows a holistic view of the predictions of the system. The operator can clearly see the estimated workload in the different motors without the need to inspect the individual plots for each GP. On the other hand, the GP contour plots (Fig.5b) present a detailed visualization of the estimations for the individual components of the system. Thanks to the linear mean prior, the GP contour plots also provide a clear view of the trend of the data w.r.t. $\mathcal{X}_{cont}$ [4]

The directed graph visualization (Fig. 5a) also displays the expected the estimated overload rate above the corresponding nodes. For improved presentation, the estimations were only displayed for the nodes with the highest workload.

Figure 6 shows the visualization for screen sizes (3.0, 1.0) when convex optimization (Eq. 13) is not used. The figure demonstrates that without enforcing the constraints in (13), the graph becomes hard to read. Some of the nodes occlude each other while others become small enough to be unreadable.

Figure 7 shows the visualizations for $\mathcal{X}_{disc} = (6.0, 1.0)$, bale moisture 20% and infeed rate 10%. The graph clearly

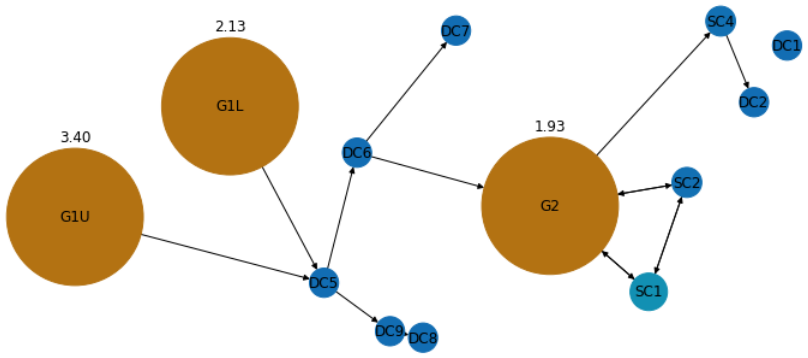

(a) Directed Graph visualization of the motors workload.

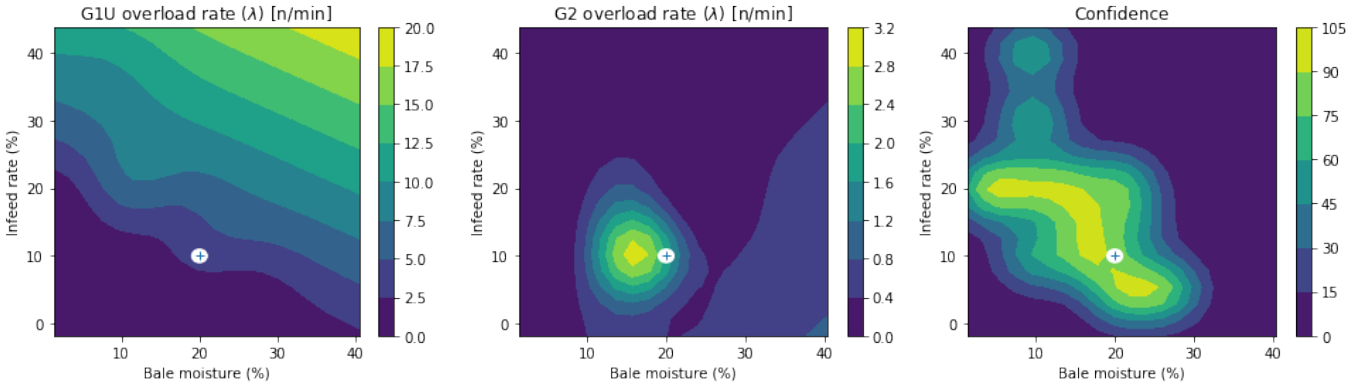

(b) GP overload rate estimations for G1U and G2 motors.

Fig. 5: Visualizations for Screen Sizes $\mathcal{X}_{disc} = (3.0, 1.0)$ and $\mathcal{X}_{cont} = (20\%, 10\%)$ a) the graph presents the predictions of the GPs in an easy interpretable way. The operator can have a holistic view of the system at a glance. The graph clearly shows that G1U, G1L and G2 motors do most of the work. The estimations of the overload rates (shown above the corresponding nodes) are only displayed for the motors with highest workload. b) The contour plot shows the estimations of the GPs over the space of $\mathcal{X}_{cont}$. The white circle represents the point $\mathcal{X}_{cont} = (20\%, 10\%)$ whose estimations were used to create the Directed Graph visualization. The confidence plot clearly shows the explored region for $\mathcal{X}_{disc} = (3.0, 1.0)$.

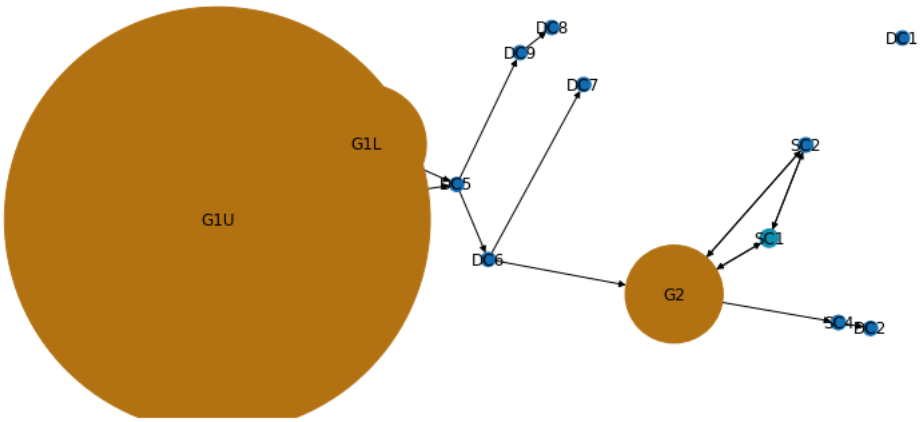

Fig. 6: Visualization directly using relevance ($\sigma(\boldsymbol{\lambda})$) without the use of the convex program. We can see that without enforcing the constraints on the scales, the visualization can potentially become cluttered and hard to read, which is specially a problem in monitoring applications where situational awareness is required.

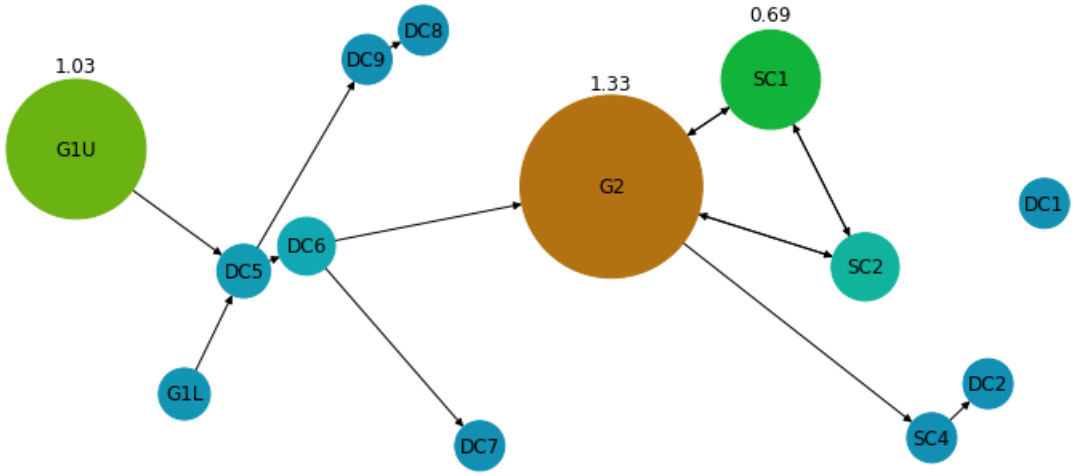

(a) Directed graph visualization.

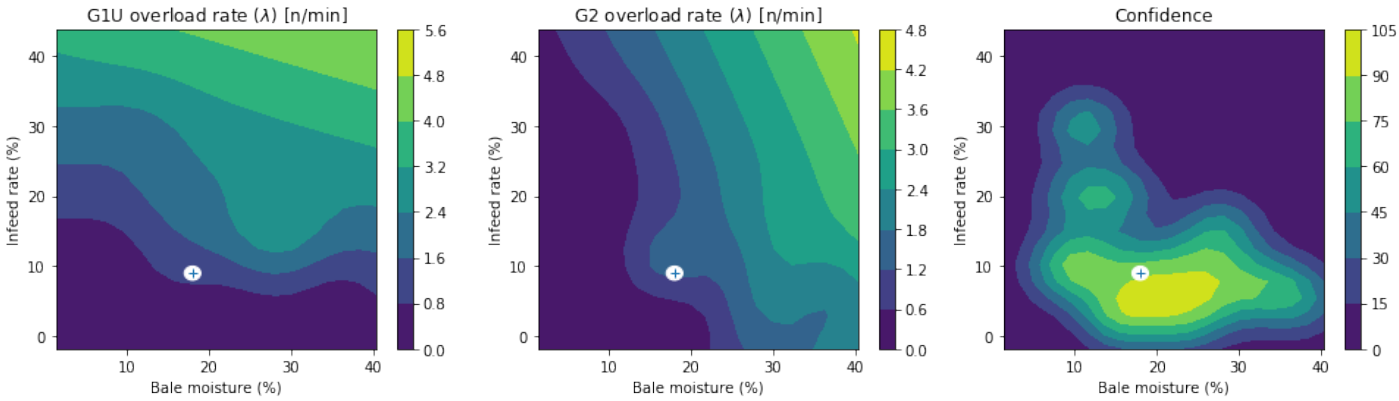

(b) GP overload rate estimations for G1U and G2 motors.

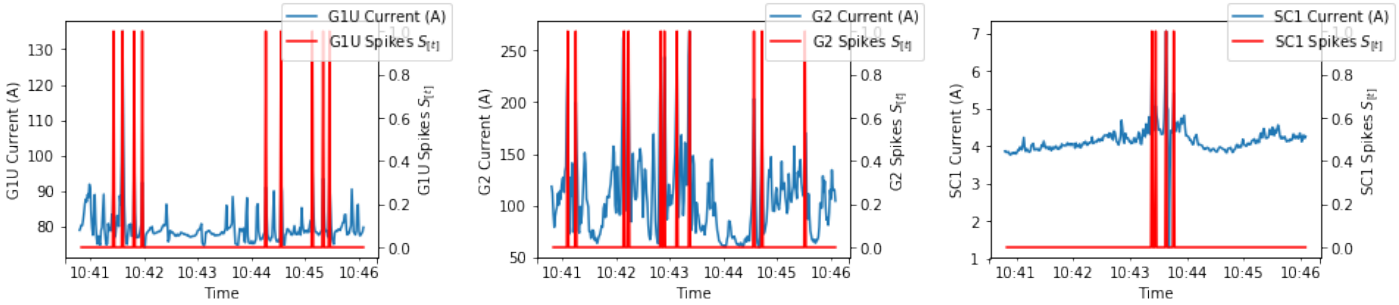

(c) Motor currents during the plant operation

Fig. 7: Visualizations for Screen Sizes $\mathcal{X}_{disc} = (6.0, 1.0)$ and $\mathcal{X}_{cont} = (18\%, 9\%)$ a) Graph visualization: in comparison with figure 5, the graph shows that the workload in G1U and G1L is significantly reduced after increasing the screen size in G1 from 3in to 6in. The graph also shows an increase of relative workload on G2 and SC1. b) GP contour plots: While the directed graph visualization presents a holistic view of the system, the contour plots of the GPs provide specific information for each one of the motors. The contour plots also show the global trend for the estimations thanks to the linear mean prior. c) The currents observed during the operation of the PDU resemble the expected behavior predicted by the GPs and visualized with the directed graph.

shows an increase of workload on $G2$, in contrast to the estimations on Fig. 5. This increase on G2 workload is a consequence of the change of Screen Size on G1.

Figure 7c shows the measured motor currents during the operation of the plant with $\mathcal{X}_{disc} = (6.0, 1.0)$, and $\mathcal{X}_{cont} = (18\%, 9\%)$ The figure shows that the behavior of the measured currents resembled the expected behavior predicted by the GPs: G2 experienced a higher overload rate, followed by G1U and SC1. The rest of the motors did not experienced overloads during the operation. We see that this behavior was clearly illustrated by the directed graph in figure 7a

Beyond the applications for knowledge discovery and data-mining, the presented methodology also serves as a powerful monitoring tool. The intuitive presentation of the predictions improves situational awareness [16] by providing valuable feedback to the operators, which can clearly see the interaction between the different processes and the potential bottlenecks.

The interpretable nature of the methodology makes it suitable for its application in controls. The prediction of the models can be used by a control algorithm to optimize the production. Understanding the models is essential to design and understand the decisions made by the control algorithm. Moreover, interpretability is essential for building trust in a control algorithm that uses the presented data-driven models for decision making [22] [23].

V. Conclusion

In this paper, we presented an interpretable data-driven methodology for estimating the workload on the different components of a biomass preprocessing plant. The methodology presents a holistic view of the system in the form of an intuitive directed graph. Furthermore, for the individual components of the plant, contour plots were used to provide detail information about the trend and confidence of the data-driven estimations.

Gaussian Processes were used to build a data-driven model for estimating the expected over-current rate for each component of the PDU system. The predictions from the GP were used to derive a relative workload measurement. A convex optimization program was used to derive a set of scales from the relative workload measurement. The scales were used to visualize a directed graph, which intuitively showed the workload on each one of the components of the system. The convex optimization program ensured a clear and uncluttered visualization of the directed graph.

Besides knowledge discovery and data-mining, the presented methodology improves situational awareness for the operation of the plant. The intuitive and interpretable presentation of the estimations makes it suitable for monitoring and control applications, where trust and synergy on the human-system interaction is required.

References

[1] X. Dai and Z. Gao, "From model, signal to knowledge: A data-driven perspective of fault detection and diagnosis," *IEEE Transactions on Industrial Informatics*, vol. 9, no. 4, pp. 2226–2238, 2013.

[2] S. Yin, S. X. Ding, X. Xie, and H. Luo, "A review on basic data-driven approaches for industrial process monitoring," *IEEE Transactions on Industrial Electronics*, vol. 61, no. 11, pp. 6418–6428, 2014.

[3] L. Jian, J. Li, and S. Luo, "Exploiting expertise rules for statistical data-driven modeling," *IEEE Transactions on Industrial Electronics*, vol. 64, no. 11, pp. 8647–8656, 2017.

[4] D. Marino, K. Amarasinghe, M. Anderson, N. Yancey, Q. Nguyen, K. Kenney, and M. Manic, "Data driven decision support for reliable biomass feedstock preprocessing," in *Resilience Week (RWS), 2017*. IEEE, 2017, pp. 97–102.

[5] L. v. d. Maaten and G. Hinton, "Visualizing data using t-sne," *Journal of machine learning research*, vol. 9, no. Nov, pp. 2579–2605, 2008.

[6] L. Van Der Maaten, "Accelerating t-sne using tree-based algorithms." *Journal of machine learning research*, vol. 15, no. 1, pp. 3221–3245, 2014.

[7] M. D. Zeiler and R. Fergus, "Visualizing and understanding convolutional networks," in *European conference on computer vision*. Springer, 2014, pp. 818–833.

[8] J. S. Tumuluru, L. Tabil, Y. Song, K. Iroba, and V. Meda, "Grinding energy and physical properties of chopped and hammer-milled barley, wheat, oat, and canola straws," *biomass and bioenergy*, vol. 60, pp. 58–67, 2014.

[9] N. Yancey, C. T. Wright, C. Conner, and J. R. Hess, "Preprocessing moist lignocellulosic biomass for biorefinery feedstocks," Idaho National Laboratory (INL), Tech. Rep., 2009.

[10] S. Paulrud, *Upgraded biofuels-effects of quality on processing, handling characteristics, combustion and ash melting*, 2004, vol. 449.

[11] J. Hess, K. Kenney, L. Ovard, E. Searcy, and C. Wright, "Commodity-scale production of an infrastructure-compatible bulk solid from herbaceous lignocellulosic biomass," *Idaho National Laboratory, Idaho Falls, ID*, vol. 6, p. 163, 2009.

[12] N. Kaliyan and R. V. Morey, "Factors affecting strength and durability of densified biomass products," *Biomass and bioenergy*, vol. 33, no. 3, pp. 337–359, 2009.

[13] D. J. Schell and C. Harwood, "Milling of lignocellulosic biomass," *Applied Biochemistry and biotechnology*, vol. 45, no. 1, pp. 159–168, 1994.

[14] P. Kumar, D. M. Barrett, M. J. Delwiche, and P. Stroeve, "Methods for pretreatment of lignocellulosic biomass for efficient hydrolysis and biofuel production," *Industrial & engineering chemistry research*, vol. 48, no. 8, pp. 3713–3729, 2009.

[15] K. L. Kenney, W. A. Smith, G. L. Gresham, and T. L. Westover, "Understanding biomass feedstock variability," *Biofuels*, vol. 4, no. 1, pp. 111–127, 2013.

[16] P. Sivils, K. Amarasinghe, M. Anderson, N. Yancey, Q. Nguyen, K. Kenney, and M. Manic, "Dynamic user interfaces for control systems," in *Human System Interactions (HSI), 2017 10th International Conference on*. IEEE, 2017, pp. 277–283.

[17] J. L. Lamothe, J. She, and X. Tan, "Cyber-physical directory with optimized visualization," in *Dependable, Autonomic and Secure Computing (DASC), 2014 IEEE 12th International Conference on*. IEEE, 2014, pp. 271–276.

[18] M. Cheung, J. She, and S. Park, "Analytics-driven visualization on digital directory via screen-smart device interactions," *IEEE Transactions on Multimedia*, vol. 18, no. 11, pp. 2303–2314, 2016.

[19] C. E. Rasmussen and C. K. Williams, "Gaussian processes for machine learning. 2006," *The MIT Press, Cambridge, MA, USA*, vol. 38, pp. 715–719, 2006.

[20] D. L. Marino and M. Manic, "Fast trajectory simplification algorithm for natural user interfaces in robot programming by demonstration," in *Industrial Electronics (ISIE), 2016 IEEE 25th International Symposium on*. IEEE, 2016, pp. 905–911.

[21] T. M. Fruchterman and E. M. Reingold, "Graph drawing by force-directed placement," *Software: Practice and experience*, vol. 21, no. 11, pp. 1129–1164, 1991.

[22] D. Gunning, "Explainable artificial intelligence (xai)," *Defense Advanced Research Projects Agency (DARPA), nd Web*, 2017.

[23] M. T. Ribeiro, S. Singh, and C. Guestrin, "Why should i trust you?: Explaining the predictions of any classifier," in *Proceedings of the 22nd ACM SIGKDD International Conference on Knowledge Discovery and Data Mining*. ACM, 2016, pp. 1135–1144.